Composite Structures 268 (2021) 113940

Contents lists available at ScienceDirect

Composite Structures

journal homepage: www.elsevier.com/locate/compstruct

Prestressed CFRP-reinforced steel columns under axial and eccentric compression

Lili Hu [a,b], Peng Feng [b,*]

[a] State Key Laboratory of Ocean Engineering, School of Naval Architecture, Ocean and Civil Engineering, Shanghai Jiao Tong University, Shanghai 200240, China
[b] Key Laboratory of Civil Engineering Safety and Durability of China Education Ministry, Department of Civil Engineering, Tsinghua University, Beijing 100084, China

ARTICLE INFO

Keywords:
Steel column
Prestress
CFRP (carbon fiber reinforced polymer)
Buckling
Stiffness

ABSTRACT

Buckling limits the slenderness of steel columns in applications. This highly efficient technology, using prestressed (PS) carbon fiber reinforced polymer (CFRP) strips to reinforce steel columns against overall buckling, can be applied in new structures or to strengthen existing structures, and is easy to construct. The buckling behavior of PS CFRP-reinforced steel columns is studied with axial and eccentric compression tests. Axial compression tests are conducted on 8 specimens with three different slenderness values (105, 140, and 200); eccentric compression tests are conducted on PS specimens of slenderness 105 with four different eccentric ratios (0, 1, 2, and 3). The buckling capacity and failure modes are obtained. The obvious reinforcing efficiency is achieved by PS CFRP; the buckling capacity of PS specimens can be increased by 19%–150%. The whole loading procedure is analyzed in detail to further explain the mechanism of PS CFRP reinforcing. Four possible critical states are determined, whose order depends on the reinforcing conditions and influences the cause of buckling, which is either material yielding or slacking of the concave side CFRP. Finally, a simplified model of reinforcing efficiency is preliminarily built based on the test results.

1. Introduction

In recent years, the amount of structural steel production has continued to increase. In China, 14 million tons were produced in 2004, and 64.8 million tons were produced in 2017; structural steel production is expected to exceed 100 million tons in 2020. The global structural steel market size was valued at USD 100.3 billion in 2019 and is estimated to register a compound annual growth rate of 5.6% from 2020 to 2027. There are numerous steel structures in the world. In addition, many steel structures, such as residences, bridges, spatial grids, high-rise structures, and long-span structures, utilize compressive steel components. According to statistical analysis, the proportion of accidents caused by the buckling of compressive steel components is the largest (approximately 33%) among all steel structure accidents. This buckling occurs quickly and leads to serious consequences. In particular, slender steel columns buckle far before reaching their ultimate strength, so buckling limits the slenderness of steel columns in applications. For high-rise buildings, long-span bridges, etc., new technology to improve the slenderness of steel columns will be very important.

Because fiber reinforced polymers (FRPs), especially carbon fiber reinforced polymers (CFRPs), have a high strength, light weight, good fatigue and corrosion resistance, applying FRPs in strengthening/reinforcing steels provides a number of meaningful advantages, which have been proven by many studies and engineering applications under different loading conditions, for example, steel columns under compression [1–6], steel beams under bending [7–9], steel components under fatigue loading [10–12], steel beams under torsion [13,14], and steel walls under shear loading [15,16].

Among the above studies, current technologies using FRP to strengthen/reinforce steel columns against overall buckling mainly include gluing FRP on the surface of the steel [17] and using FRP tubes with filling material around steel [5,6], which are proven to be useful. However, the improvement of gluing FRP is relatively limited due to the debonding of FRP before the buckling of steel. In this situation, a new technology of applying prestressed (PS) CFRP to reinforce steel columns has been proposed [18], which achieves a good reinforcing efficiency, is easy to manufacture and is lightweight.

The mechanical system of PS CFRP-reinforced steel columns is similar to that of PS stayed steel columns proposed by Chu and Berge [19],

* Corresponding author.
E-mail address: fengpeng@tsinghua.edu.cn (P. Feng).

https://doi.org/10.1016/j.compstruct.2021.113940
Received 23 August 2020; Accepted 28 March 2021
Available online 31 March 2021

which comprise a slender steel column and an external pretensioned steel cable-stay system. Smith et al. [20] found that a PS stayed column has two buckling modes under ideal conditions (i.e., single-wave symmetric and double-wave antisymmetric modes). Hafez et al. [21] theoretically revealed the relationship between the prestress value and buckling capacity of an ideal PS stayed column. Saito and Wadee [22] studied the postbuckling behavior of a PS stayed column in detail. In addition, some experiments were conducted recently to study the buckling behavior of PS stayed columns with varied parameters (e.g., Serra et al. [23]). In general, PS stayed columns exhibit a good compressive behavior and are lightweight.

Compared with that of PS stayed columns, the application field of PS CFRP-reinforced steel columns is wider because this novel technology can be used directly in new structures or to strengthen existing structures, and the high-performance CFRP material improves the performance of the column because CFRP has a large elastic modulus range (100–500 GPa), a high strength (usually greater than 2000 MPa), and a constant axial tensile stiffness that does not decrease during prestressing. However, limited studies have been performed on the buckling behaviors of PS CFRP-reinforced steel columns. Thus, this paper describes a series of experimental tests, detailed analysis and simple modeling to study the buckling behavior of this composite component, which can be used as a typical and basic element of steel structures. The buckling capacity, failure mode, bending stiffness, and reinforcing efficiency of the PS CFRP-reinforced steel columns under axial and eccentric compressive loadings are obtained. The physical state change during the loading procedure is also revealed, based on which different causes of buckling are identified, contributing to a better understanding of the buckling mechanism. A simple model considering the influential tendency of different parameters is built, providing valuable references for future design guidelines.

2. PS CFRP reinforcing technology

According to an earlier paper [18], PS CFRP reinforcing is suitable for commonly used symmetric steel section forms, steel section dimensions and steel grades and efficient for steel columns of large slenderness. Taking an example of reinforcing overall buckling behavior of the weak axis of an I-section steel column, the reinforcing system includes CFRP, an anchorage and a prestressing chair, as shown in Fig. 1(a). The implementation steps are summarized in Fig. 1(b). Step 1: Weld the prestressing chairs on the midspan of the steel column. Step 2: Place the CFRP strips across the prestressing chairs and along the length of the steel column, then anchor the two ends of the CFRP and the two ends of the steel column together. Step 3: Stretch the CFRPs by rotating the bolts of the prestressing chairs.

Key geometric parameters of the PS CFRP-reinforced steel column are defined in Fig. 1(b). The length of the steel column is L; the anchoring length at one end is L_a, both of which do not change due to prestressing. The geometric parameters before the prestressing of CFRP are as follows: the initial supporting length is a_0; the initial length of the CFRP is $L_{P,0} + 2L_a$. The geometric parameters after the prestressing of the CFRP are as follows: the (final) supporting length is a; the final length of the CFRP is $L_P + 2L_a$; the angle between the CFRP and the axis of the steel column is α, which has a positive relationship with the ratio of a to L. The relationships of the above parameters are shown in Eqs. (1)–(3), where E_P and A_P are the elastic modulus and section area of the CFRP, respectively.

Key mechanical parameters are defined as follows. The external compressive force is P. The prestress force of the CFRP is T, and its initial value before loading is T_i. Subscripts l and r represent the left side and right side, respectively. The two forces transferred from the PS CFRP to the steel column are the transverse force S (from Eq. (4)) and vertical force N (from Eq. (5)).

$$T_i = (L_P - L_{P,0})/L_{P,0} \times E_P A_P \tag{1}$$

$$L_P = 2\sqrt{(L/2 - L_a)^2 + a^2} \tag{2}$$

$$L_{P,0} = 2\sqrt{(L/2 - L_a)^2 + a_0^2} \tag{3}$$

$$S = 2T_r \sin\alpha - 2T_l \sin\alpha \tag{4}$$

$$N = (T_r + T_l)\cos\alpha \tag{5}$$

The reinforcing mechanism includes three aspects. (1) Firstly, high-strength and elastic CFRP is placed outside the steel, which is beneficial to improve the cross-section bearing capacity of the member. (2) Secondly, as shown in Fig. 1(c), when P is applied, the PS CFRP introduces two forces (N and S) to the steel column. S provides an effective lateral support to resist buckling, and N weakens the member. Therefore, there is an optimal CFRP prestress that makes the improvement by S more significant than the weakening by N to maximize the buckling capacity of the steel column. (3) After reinforcement, the initial geometric imperfections of the steel column along the length can be effectively reduced. Since the overall buckling of the steel column is greatly affected by this initial geometric imperfection, the reinforcing system can further enhance the stability of the steel column [24].

This PS CFRP reinforcing technology for steel columns is expected to have the following five advantages. (1) The reinforcing efficiency will be significant because the reinforcing system delays the lateral displacement and effectively avoids the debonding of the CFRP before the steel column buckles, thereby fully utilizing the high strength of the CFRP, and the initial imperfections after the reinforcement can be reduced. (2) The reinforcing material is only CFRP, and no filling material is needed; the density of the CFRP is low, so there is a very light weight added to the original structure after reinforcement. (3) The reinforcing material CFRP has good corrosion resistance and fatigue resistance without requiring special treatments. (4) The construction process is convenient. Specifically, CFRP is easy to transport due to its light weight; the anchoring is convenient and efficient because no failure of the anchorages occurs before the buckling of the steel column; the prestressing of the CFRP is convenient and is achieved by a prestressing chair without any additional device. (5) When reinforcing the weak axis of the I-section column, the CFRP is stretched from the steel column web. If the final supporting length a is less than half of the flange width of the I-section, the steel column section will not be enlarged after reinforcement, so the reinforcement does not occupy extra space.

3. Experimental program

To obtain the buckling behaviors of PS CFRP-reinforced steel columns, experimental tests are performed; the experimental design is described in this part, and the corresponding test results are presented and analyzed in Part 4.

3.1. Material properties and sections

Q690 and Q420 steels are used because steel strength is a study parameter. Through a standard material test [25], stress-strain curves of the two types of steels are obtained, as shown in Fig. 2. Based on the results of the abovementioned material tests and previous studies [18], the material properties of the steel and CFRP are summarized in Table 1.

The sizes of the steel and CFRP sections are shown in Fig. 3. The areas of the steel section and CFRP section are denoted A_s and A_P, respectively. According to the Chinese standard for design of steel structures [26], the width-to-thickness ratio of the steel web and flange are set to ensure that local buckling will not occur before overall buckling. The configurations of the prestressing chair and anchorage are the same as in a previous paper [18].

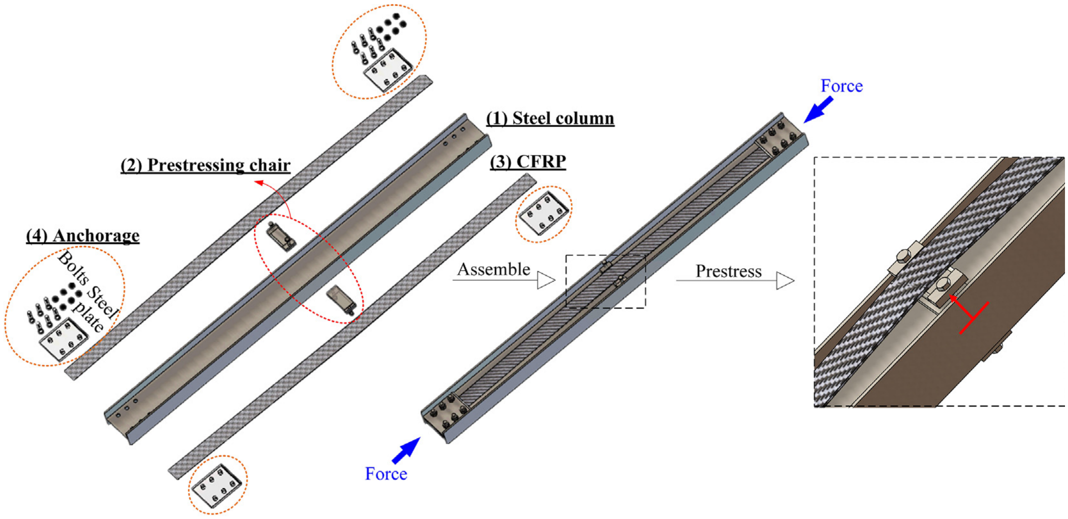

(a) Schematic diagram

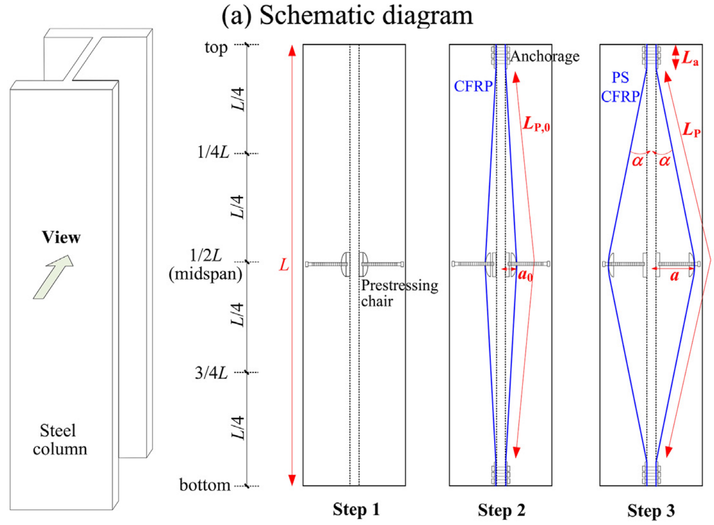

(b) Implementation steps and definition of geometric parameters

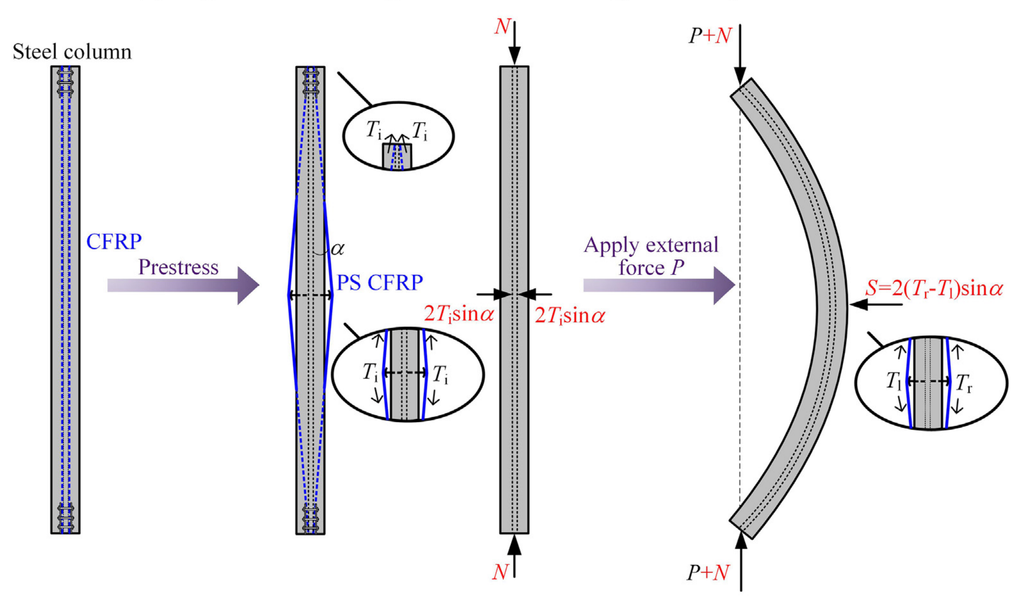

(c) Mechanical system

Fig. 1. Steel columns reinforced by PS CFRP strips [18].

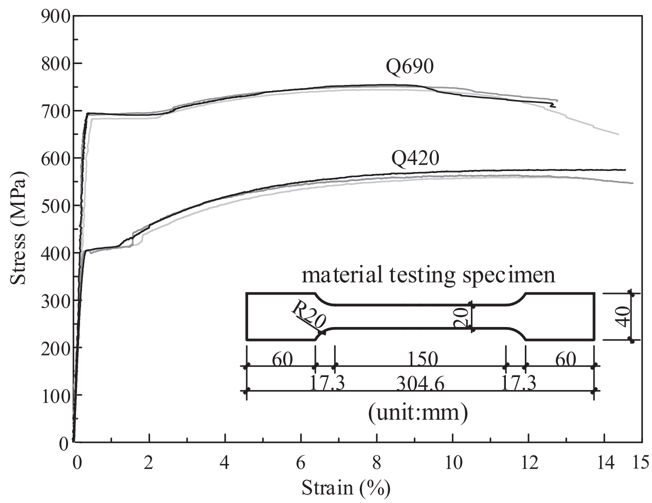

Fig. 2. Stress-strain curves of the steels.

Table 1
Material properties of the steel and CFRP.

Material	Yield point (MPa)	Ultimate strength (MPa)	Elastic modulus (GPa)
Q690 steel	$f_y = 682$	$f_{u,s} = 765$	$E_s = 206$
Q420 steel	$f_y = 401$	$f_{u,s} = 564$	$E_s = 206$
CFRP	–	$f_{u,P} = 2450$	$E_P = 171$

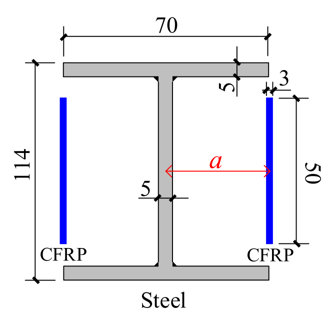

Fig. 3. Steel and CFRP sections (unit: mm).

3.2. Test specimens

This test included two groups to study the buckling behavior under axial and eccentric compressive loadings, namely, the axial loading and eccentric loading groups. All the specimens are shown in Table 2. I represent the I-section of steel, and the number following I represents the design slenderness λ. The symbol U represents the unreinforced specimen (i.e., pure steel column); S represents the non-PS CFRP reinforced specimen, which has no prestressing chairs; PS represents the PS CFRP-reinforced specimen, as shown in Fig. 4. L is the measured length of the steel column specimens; L_c is the calculation length, which is the sum of L and the thickness of the 2 end plates (i.e., 20 mm) and twice the distance from the hinge to the end plate (i.e., 50 mm). Because the prestressing chair at the midspan caused the stress concentration in the CFRP, the initial prestress of the CFRP measured at $1/4L$ or $3/4L$ is considered the initial prestress T_i for subsequent analysis. The anchorage length L_a of the I105 series and I140 series is 130 mm, and that of the I200 specimens is 200 mm, ensuring sufficient anchorage strength.

For the axial loading group, there are three series (i.e., the I105 series, I140 series, and I200 series) corresponding to three different design slenderness values λ. For every series, there are 2 or 3 forms (i.e., among U, S, and PS). The cross-sectional dimensions of the specimens are the same, so the U and S specimens are reference specimens for the PS specimens. The design lengths of the I105, I140, and I200 series are 1610, 2147, and 3067 mm, respectively. The range of T_i/A_P is 123 MPa to 302 MPa, which is 5.0%–12.3% of the CFRP strength f_P. The initial supporting length a_0 is 0. The supporting length a is 41, 70, and 78 mm for I105-PS, I140-PS, and I200-PS; thus, the corresponding values of a/L are 2.5%, 3.2% and 2.5%, respectively.

In the eccentric loading group, there are 4 PS specimens, including one axial compression specimen (I105-PS-e0) for reference and three eccentric compression specimens (I105-PS-e1, I105-PS-e2 and I105-PS-e3) corresponding to three different eccentric ratios e/r (1, 2, and 3). The design slenderness of this group is 105; the design steel column length is 1610 mm; the initial supporting length a_0 is 0. The supporting length a of this group is kept almost constant so that the value of a/L is almost constant (ranging from 3.2% to 3.4%), and the small difference is caused by construction; thus, the corresponding initial prestress of the CFRP T_i/A_P ranges from 150 MPa to 220 MPa, which is 6.1% to 9.0% of the CFRP strength f_P. The changing parameter of these specimens is the eccentric ratio e/r, in which e is the eccentricity and r is the radius of gyration of the steel section. The r value selected for of all the specimens is 15.5 mm. For the specimen naming scheme, e1, e2 and e3 represent eccentric ratios of 1, 2 and 3, respectively, corresponding to eccentricities of 15 mm, 31 mm, and 46 mm, respectively.

3.3. Loading and measurement

The measurement device used in the axial compression test is presented in Fig. 5. The boundary conditions of all the specimens are set as a one-way hinge support for the two ends, which ensures that the column can buckle around the weak axis of the I-section steel column. Six vertical displacement meters (e.g., DT1, DT2, and DT11-14) and 3

Table 2
Test specimens.

Specimen		λ	Reinforcing method	L (mm)	L_c (mm)	T_i/A_P (MPa)	A (mm)	a/L	e/r	Steel
Axial loading group	I105-U	105	-	1617	1687	-	-	-	0	Q690
	I105-S	105	by non-PS CFRP	1620	1690	0	0	0	0	Q690
	I105-PS	105	by PS CFRP	1619	1689	123	41	2.5%	0	Q690
	I140-U	140	–	2148	2218	–	–	–	0	Q690
	I140-S	140	by non-PS CFRP	2150	2220	0	0	0	0	Q690
	I140-PS	140	by PS CFRP	2154	2224	302	70	3.2%	0	Q690
	I200-S	200	by non-PS CFRP	3070	3140	0	0	0	0	Q690
	I200-PS	200	by PS CFRP	3065	3135	146	78	2.5%	0	Q690
Eccentric loading group	I105-PS-e0	105	by PS CFRP	1621	1691	190	53	3.2%	0	Q420
	I105-PS-e1	105	by PS CFRP	1615	1685	220	55	3.4%	1	Q420
	I105-PS-e2	105	by PS CFRP	1616	1686	160	53	3.3%	2	Q420
	I105-PS-e3	105	by PS CFRP	1619	1689	150	51	3.2%	3	Q420

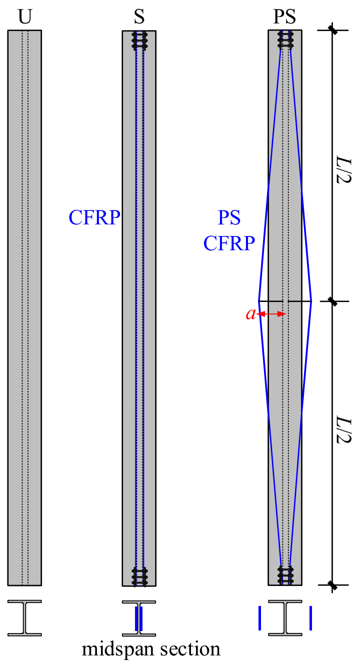

Fig. 4. Schematic diagrams of the three studied forms (U, S, and PS).

horizontal displacement meters (e.g., DT5-DT6 and DT15) were set up. Lateral deformations were measured by DT5 and DT6; the vertical deformation was measured by DT13 and DT14; the rotation angles of the top hinge and bottom hinge were measured by meters DT1 and DT2 and meters DT11 and DT12, respectively; and the out-of-plane displacement at the midspan was measured by DT15. In total, 24 strain gauges were placed on three steel sections (sections A-A, C-C, and E-E), and 4 strain gauges were placed on two CFRP sections (sections B-B and D-D), because stress concentration occurs around the prestressing chair and the anchorages. To leave space for the displacement meters, sections A-A to E-E are approximately 10 mm from the corresponding locations (0, $1/2L$, $1/4L$, $3/4L$, and L locations). Specifically, for the PS specimens, DT7 and DT8 are added to measure the vertical displacements of the left and right prestressing chairs. In addition, for I200-PS, a high-precision noncontact method, based on image speckle recognition technology, was applied to measure the displacements at important points in the steel column during the loading procedure [27].

For the eccentric compression test, the loading device is basically the same as described the above. The only difference is the design of the end plate to achieve eccentric loading, as shown in Fig. 6. Through this design, the rotation axis of the one-way hinge is away from the central axis of the steel section by a distance e. For specimens I105-PS-e1, I105-PS-e2 and I105-PS-e3, e is designed to be 15, 31 and 46 mm, respectively. The measurements are performed with the displacement meters and strain gauges, which are arranged the same as those in Fig. 5.

4. Experimental results and analysis

4.1. Buckling capacity and failure mode

4.1.1. Buckling capacity

The buckling capacity is P_b, which is also the loading bearing capacity of the buckling members. The test results of the buckling capacities are shown in Table 3 and Figs. 7 and 8. For the buckling capacities of the reinforced specimens including the S and PS specimens, $P_{b,s}$ is used; for that of the U specimens, $P_{b,u}$ is used.

For the axial loading group, the following results are obtained. For the I105 series, the buckling capacity of I105-S is only 9% higher than that of I105-U; the buckling capacity of I105-PS is 36% higher than that of I105-U. For the I140 series, the buckling capacity of I140-S is 10% higher than that of control specimen I140-U, and the buckling capacity of I140-PS is 150% higher than that of I140-U. For the I200 series, the buckling capacity of I200-U was obtained by the finite element method (FEM) with a 0.1%L initial imperfection, for which the finite element model was presented in an earlier paper [18]. The buckling capacity of I200-S is 5% lower than that of I200-U, while the buckling capacity of I200-PS is 118% higher than that of I200-U. For the eccentric loading group, the results of unreinforced specimens are calculated with the FEM using the model presented in an earlier paper [18] with an initial imperfection of 0.02%L according to real measurements [24]. As the eccentricity increases, the buckling capacity of the specimens decreases, and the improvement in the buckling capacity of the specimens generally increases from 19% to 36%, which means that PS CFRP can decrease the initial eccentricity sensitivity of steel columns.

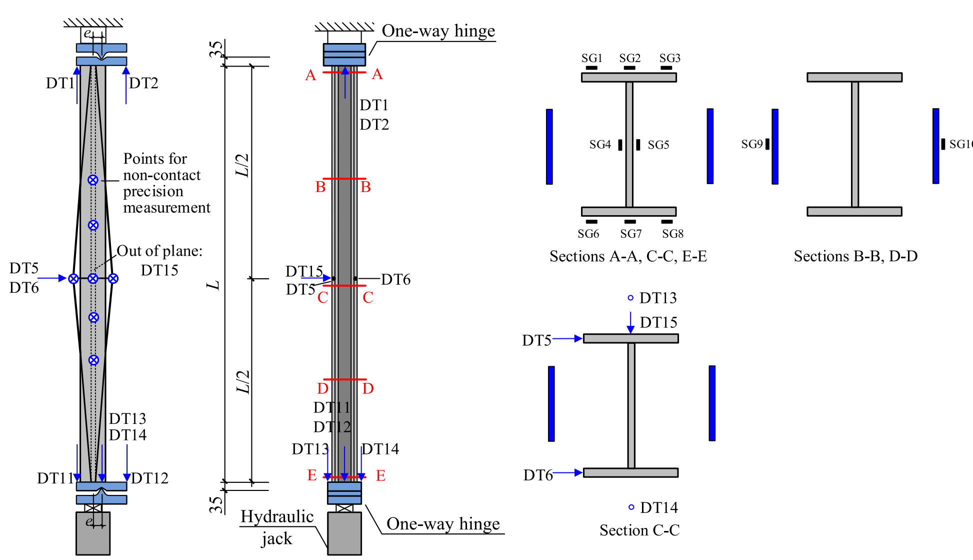

Fig. 5. Loading and measurement device.

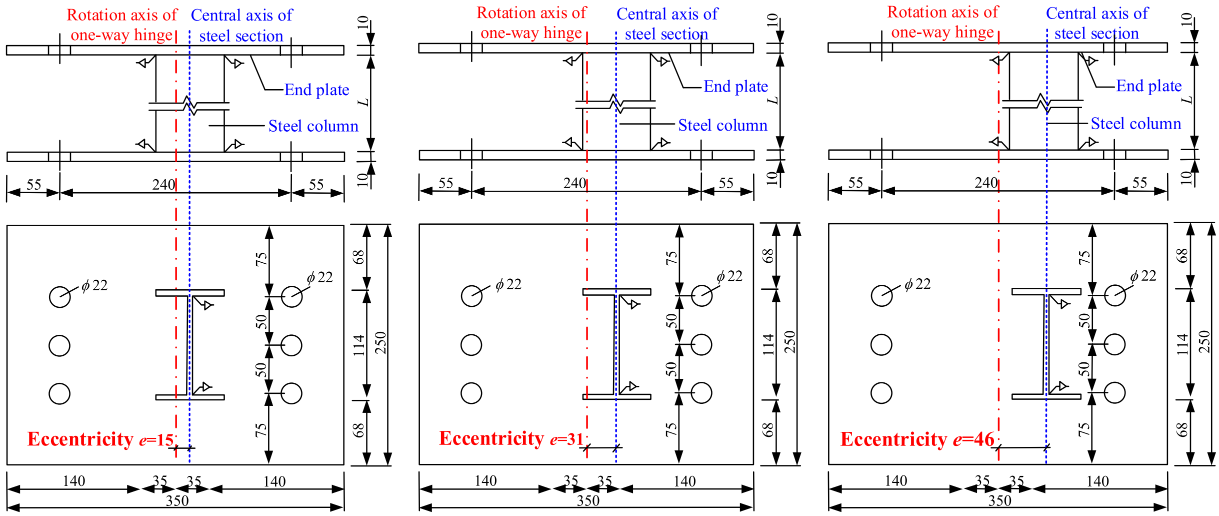

Fig. 6. Design of the end plate to achieve eccentric loading (unit: mm).

Table 3
Test results of buckling capacity and bending stiffness.

Specimen		P_b (kN)	$P_{b,s}/P_{b,u}$	k_b (kN/mm)	$k_{b,s}/k_{b,u}$	P_b/P_E	P_b/P_d
Axial loading group	I105-U	183	1.00	37.5	1.00	0.90	1.22
	I105-S	199	1.09	20.0	0.53	0.98	1.33
	I105-PS	249	1.36	56.0	1.49	1.22	1.66
	I140-U	103	1.00	16.3	1.00	0.87	1.11
	I140-S	113	1.10	16.3	1.00	0.96	1.21
	I140-PS	258	2.50	Infinite	Infinite	2.19	2.77
	I200-U(FEM)	56	1.00	4.5	1.00	0.95	1.14
	I200-S	53	0.95	7.7	1.71	0.90	1.08
	I200-PS	122	2.18	15.0	3.33	2.07	2.49
Eccentric loading group	I105-U-e0(FEM)	176	1.00	44.0	1.00	–	–
	I105-U-e1(FEM)	98	1.00	5.8	1.00	–	–
	I105-U-e2(FEM)	67	1.00	3.8	1.00	–	–
	I105-U-e3(FEM)	53	1.00	2.7	1.00	–	–
	I105-PS-e0	210	1.19	50.4	1.14	–	–
	I105-PS-e1	116	1.18	8.0	1.40	–	–
	I105-PS-e2	90	1.34	5.0	1.33	–	–
	I105-PS-e3	72	1.36	3.8	1.41	–	–

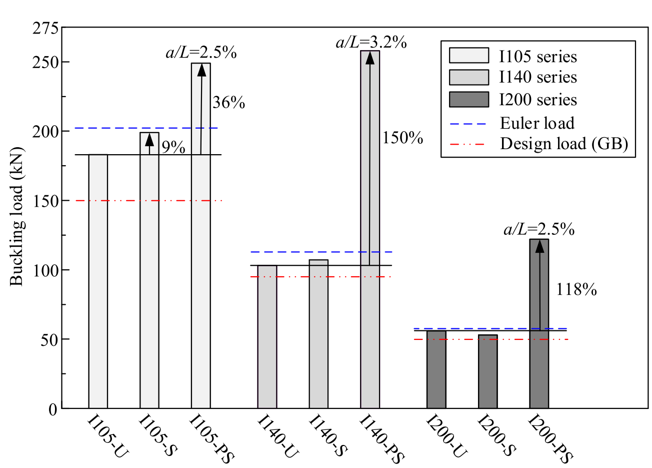

Fig. 7. Buckling capacities of the specimens in the axial loading group.

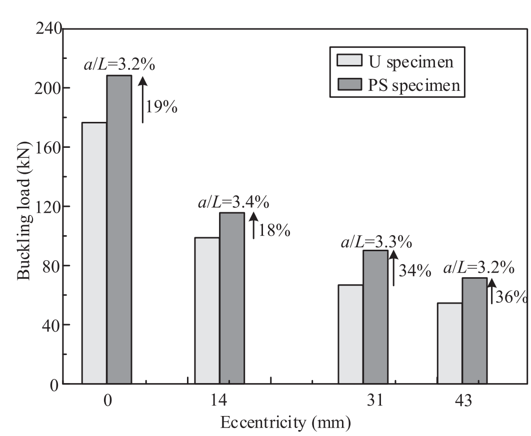

Fig. 8. Buckling capacities of the specimens in the eccentric loading group.

The reinforcing efficiency is defined as the ratio of $P_{b,s}$ to $P_{b,u}$. Based on the above results, it can be concluded that non-PS CFRP without prestressing chairs cannot significantly enhance the buckling capacity. In some cases, due to the effect of the initial imperfection, the buckling capacity of the S specimen can even be lower than that of the U specimen. The improvement in the PS CFRP is pronounced because its reinforcing efficiency ($P_{b,s}/P_{b,u}$) ranges from 1.36 to 2.50 under axial compression and 1.19 to 1.36 under eccentric compression.

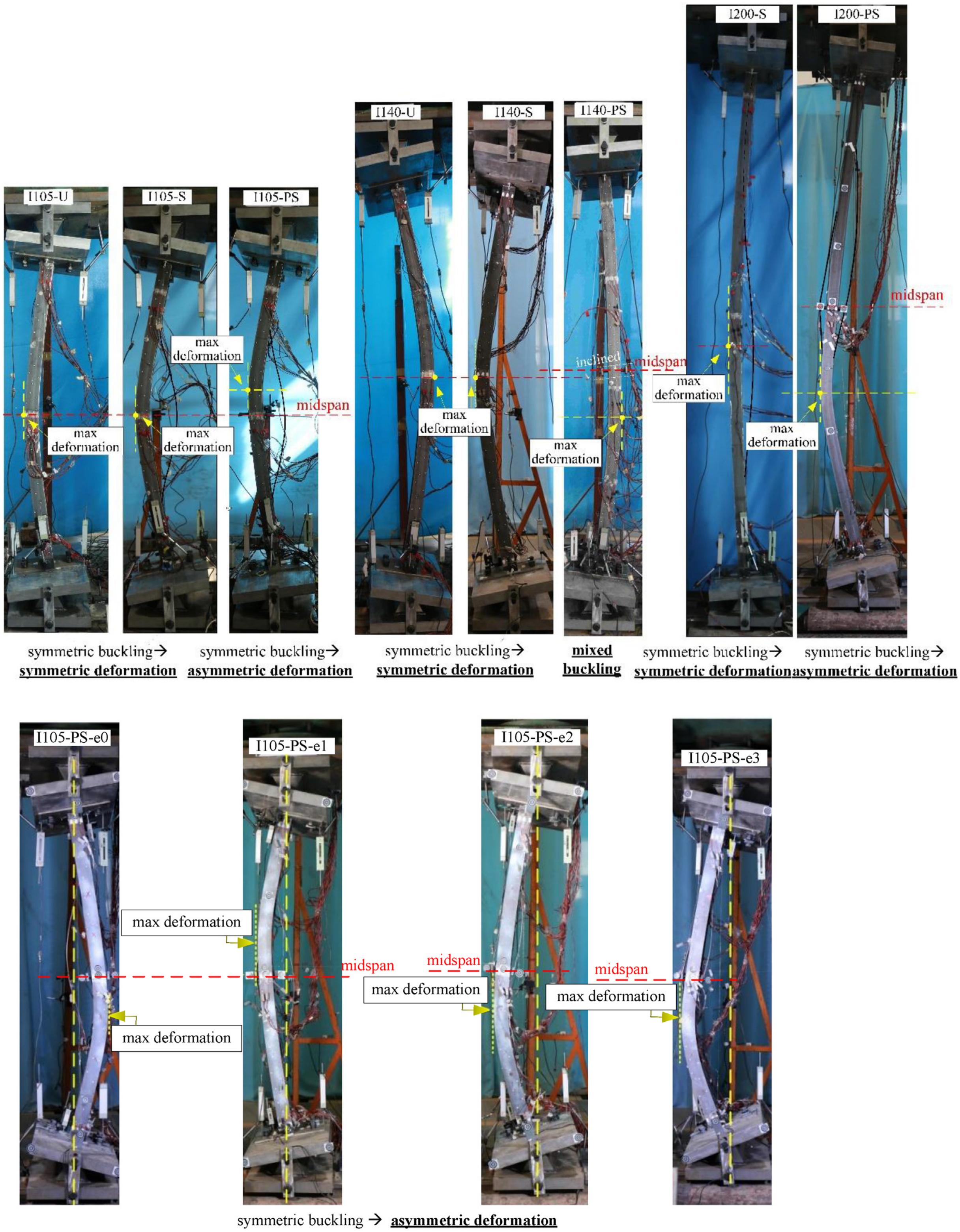

Fig. 9. Failure modes.

In addition, for specimens in the axial loading group, P_E is the Euler load of the weak axis of the pure steel column, and P_d is the corresponding design load according to the Chinese standard for design of steel structures [26]. The calculated design loads for I105, I140 and I200 series under axial compression are 204, 118 and 59 kN, respectively; the Euler loads for I105, I140 and I200 series are 150, 93 and 49 kN, respectively. The ratio of $P_{b,s}$ to P_E ranges from 1.22 to 2.19, and the ratio of $P_{b,s}$ to P_d ranges from 1.66 to 2.77 under axial compression. The large ratios of $P_{b,s}$ to P_E or P_d also imply a good reinforcing efficiency provided by PS CFRP.

The boundary conditions of the above specimens in the direction of the strong axis are fixed at both ends. The slenderness values of the

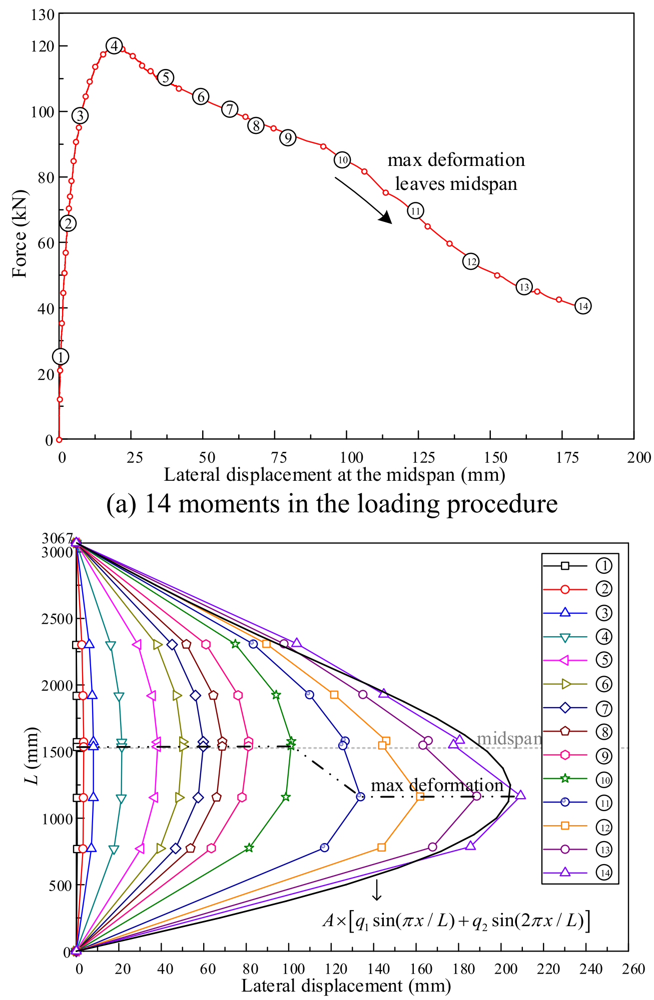

(a) 14 moments in the loading procedure

(b) Lateral displacements along steel column length L

Fig. 10. Lateral displacements along the steel column length of I200-PS at different moments.

strong axes of the I105 series, I140 series and I200 series are 43.0, 56.6 and 79.9, respectively, and the design loads are 477, 367 and 246 kN, respectively. The buckling capacity of the weak axis after reinforcing is closer to that of the strong axis.

4.1.2. Failure mode

For all the specimens, the measured out-of-plane displacements at the midspan are very small (less than 0.3 mm before buckling) compared with the lateral displacement at the same loading moment. Thus, all the specimens experienced in-plane buckling, as expected. The failure modes of all the specimens are shown in Fig. 9. For all the specimens, the CFRP does not rupture or debond before buckling occurs. However, there is a large difference in the failure modes of the U, S and PS specimens.

For the U and S specimens, the buckling modes are typical symmetric overall buckling. The lateral deformation when buckling is triggered and after buckling presents a sine wave distribution, and the maximum lateral displacement occurs at the midspan. For the PS specimens, two situations arise. (1) For I105-PS and I200-PS and all the specimens in the eccentric loading group, a symmetrical buckling mode occurs with symmetrical deformation when buckling is triggered, but asymmetrical deformation occurs after buckling. The specific manifestations are as follows: the maximum lateral deformation is not at midspan, and the prestressing chairs are inclined. (2) The I140-PS specimen experiences a mixed buckling mode between the symmetric and antisymmetric buckling modes, that is, its deformation when buckling is triggered is asymmetrical.

Noncontact high-precision measurement is used to track the deformation of I200-PS along the column length for 14 moments during the loading procedure, as shown in Fig. 10(a), and the lateral displacements corresponding to the 14 moments are shown in Fig. 10(b). When buckling occurs (typical time 4), the deformation along the length of the column is still symmetric, but with the development of deformation, the maximum deformation shifts from the midspan to non-midspan at typical time 11; at this moment the deformation can be described as a linear combination of a single sine wave and double sine wave (i.e., $A\times[q_1\sin(\pi x/L)+q_2\sin(2\pi x/L)]$), where A is 230, q_1 is 0.83, and q_2 is 0.17. Therefore, the mixed deformation of I200-PS at typical time 11 is the sum of the 83% symmetric and 17% antisymmetric buckling modes.

In addition, the symmetric buckling and later asymmetric deformation of the I105-PS and I200-PS specimens can be proven by Fig. 11. Only when asymmetric deformation occurs will the horizontal prestressing chair become inclined. In Fig. 11, before buckling, the vertical displacement at the end of the prestressing chair is relatively small, so the buckling mode is symmetric; however, after buckling occurs, the vertical displacement at the end of the prestressing chair becomes large, so asymmetric deformation occurs after buckling.

The reason that I140-PS has mixed buckling but other PS specimens have symmetric buckling is explained as follows. According to previous literature [28–30], prestressing chairs constrain the translation

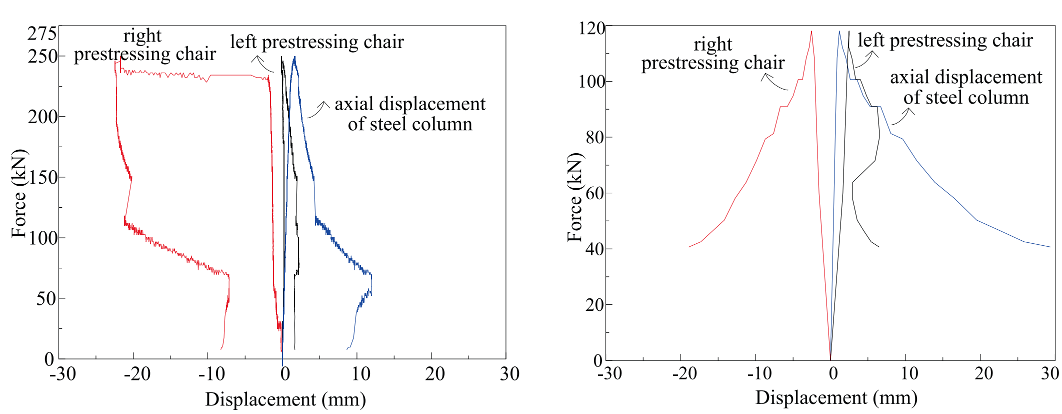

(a) I105-PS

(b) I200-PS

Fig. 11. Force and vertical displacement at the end of the prestressing chair.

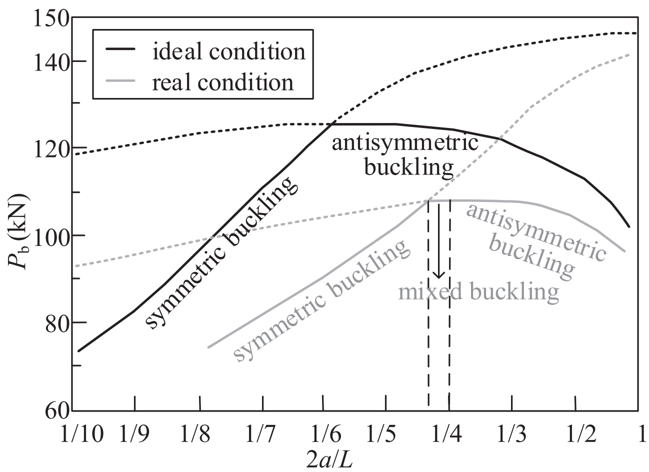

Fig. 12. Conditions of symmetric, mixed and antisymmetric buckling [28–30].

and rotation of the midspan of the steel column. When the rotation constraint is stronger, the PS specimens will undergo symmetric buckling; when the translation constraint is stronger, the PS specimens will undergo antisymmetric buckling; when the above two constraints are equally strong, the PS specimens will undergo mixed buckling between symmetric and antisymmetric buckling. Thus, as shown in Fig. 12, with a certain value of *L*, when the supporting length *a* is small, the translation constraint of the prestressing chair is small, so symmetric buckling occurs. When *a* increases, the symmetric buckling capacity will increase until it reaches the antisymmetric buckling capacity, and the failure mode changes from symmetric to mixed buckling mode. In this situation, continuing to increase *a* will make the buckling mode transition from mixed buckling to antisymmetric buckling. For the I140-PS specimen, the ratio of the supporting length to steel column length is large enough (i.e., 3.2%), so the mixed buckling occurs; however, for other PS specimens, this ratio is small, so symmetric buckling occurs.

4.2. Load-deformation curves

For the axial loading group, the force-lateral displacement curves are shown in Fig. 13; the force-axial displacement curves are shown in Fig. 14. For the eccentric loading group, the force-lateral displacement curves are shown in Fig. 15; the force-axial displacement curves are shown in Fig. 16.

Based on the "farthest point method" [31], yield points of all the specimens are obtained. The bending stiffness of a specimen can be defined as the secant slope of the yield point. The bending stiffness corresponding to the U specimen is $k_{b,u}$; the bending stiffness corresponding to the S and PS specimens is $k_{b,s}$. The calculated bending stiffnesses are shown in Table 3.

For the axial loading group, the following results are obtained. For the I105 series, the bending stiffness of I105-S is only 0.53 of I105-U; the bending stiffness of I105-PS is 49% higher than that of I105-U. For I140 series, the bending stiffness of I140-S is the same as that of control specimen I140-U, and the bending stiffness of I140-PS is very large (i.e., the lateral displacement is almost zero before 68%P_b). For the I200 series, the bending stiffness of I200-S is 71% higher than that of I200-U, and I200-PS achieves a bending stiffness 233% higher than that of I200-U. Additionally, the axial stiffness is not significantly improved by the non-PS CFRP under axial compressive loading.

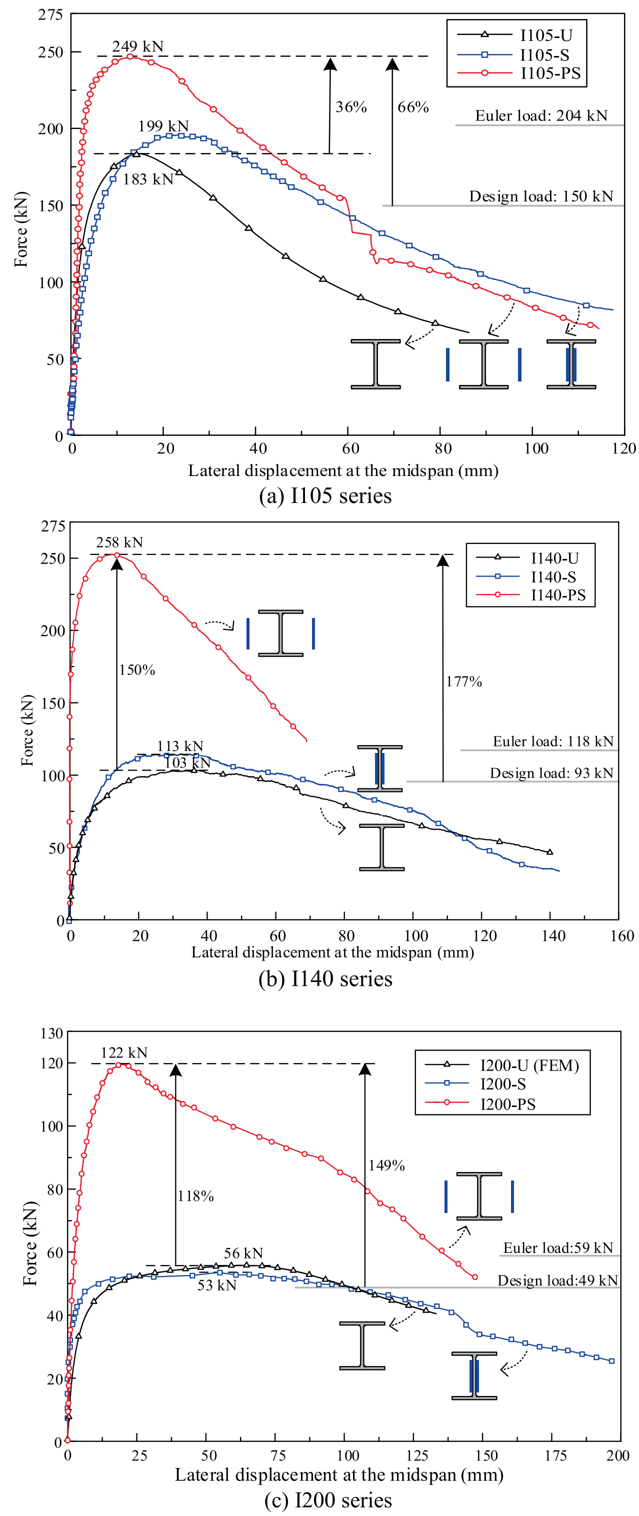

Fig. 13. Force-lateral displacement curves of specimens in the axial loading group.

For the eccentric loading group, as the eccentricity increases, the bending stiffness and axial stiffness of the specimens decrease, and the PS CFRP can improve the bending stiffness by 14%–41%.

Thus, combining these results with those in Part 4.1, PS CFRP reinforcing can significantly improve the buckling capacity and bending stiffness of steel columns under axial and eccentric compression.

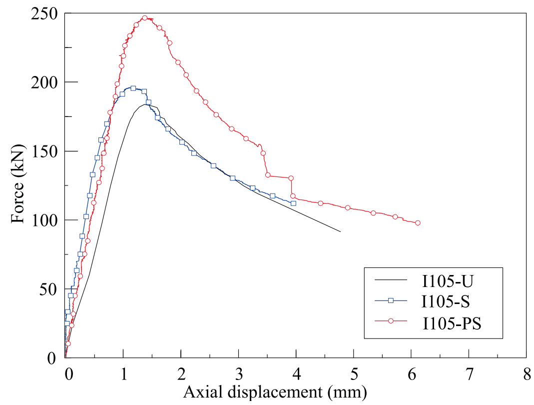

(a) I105 series

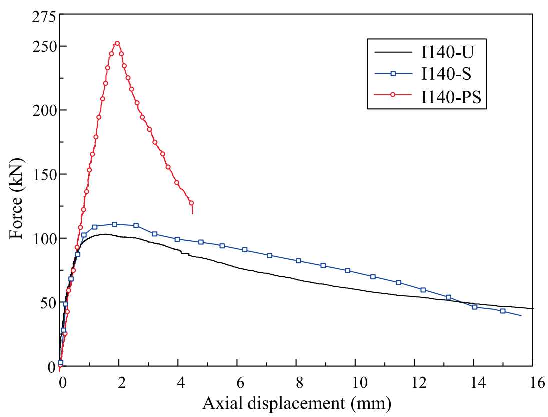

(b) I140 series

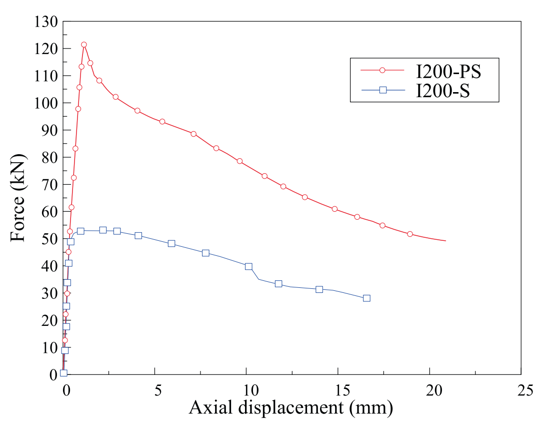

(b) I200 series

Fig. 14. Force-axial displacement curves of specimens in the axial loading group.

4.3. Critical states

To study the critical states of the column, a detailed analysis of the development of the CFRP and steel stress is first studied.

Tensile stress is set as positive. Because the CFRP strip is thin, it is supposed that the stress distribution of the CFRP is uniform. Thus, the CFRP stress away from the prestressing chair is set as σ_P. Its initial value is $\sigma_{PS,P}$, which equals T_i/A_P (≥ 0). When external force P is applied, σ_P is the sum of the initial prestress ($\sigma_{PS,P}$), stress change due to the axial compression ($\Delta\sigma_{c,P} < 0$) and the stress due to the lateral deformation of the column ($\Delta\sigma_{d,P}$: convex side, >0; concave side, <0), as shown in Eq. (6).

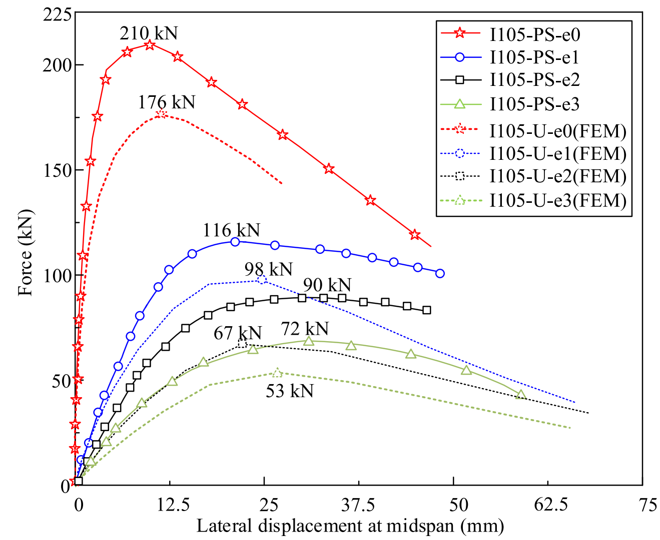

Fig. 15. Force-lateral displacement curves of specimens in the eccentric loading group.

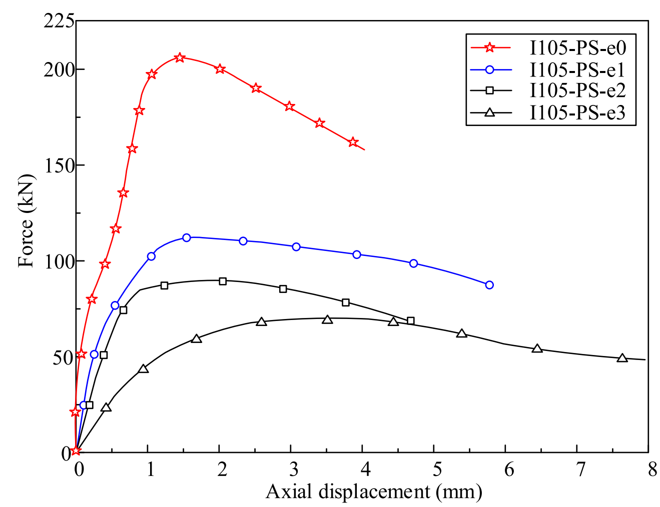

Fig. 16. Force-axial displacement of specimens in the eccentric loading group.

$$\sigma_P = \sigma_{PS,P} + \Delta\sigma_{c,P} + \Delta\sigma_{d,P} \quad (6)$$

Correspondingly, the steel stress σ_s is the sum of the precompression stress provided by the PS CFRP ($\sigma_{PS,s} = N/A_s < 0$), stress change due to the axial compression $\Delta\sigma_{c,s}$ (<0) and stress change due to the lateral deformation of the column ($\Delta\sigma_{d,s}$: convex side, >0; concave side, <0).

For the S and PS specimens, there are three objects to consider (the steel column, convex side CFRP and concave side CFRP), and there are prestressing procedure and loading procedure. During the loading procedure, there are two possible deformation phases: (1) compressive deformation phase, when the major deformation is compression so that the CFRP stress on both sides decreases or remains zero; and (2) lateral bending phase, when the major deformation is lateral bending deflection so that the convex side CFRP stress increases but the concave side CFRP stress decreases or remains zero.

For the PS specimens, there are 4 possible critical states throughout the loading procedure: (1) at the beginning of the lateral bending phase, (2) slacking of the concave side CFRP, (3) overall buckling, and (4) steel column edge yielding. For the S specimens, only critical states (1), (3) and (4) are possible. More details are shown as follows.

4.3.1. S specimens

For specimens I105-S, I140-S and I200-S, the concave side CFRP is slack, and the measured convex side CFRP stress-lateral displacement curves are shown in Fig. 17. The CFRP stresses at the 1/4L and 3/4L locations are very similar; thus, only one value is presented. Without the prestressing chair and prestressing step, $\sigma_{PS,P}$ equals 0. At the beginning, there is a compressive deformation phase; thus, $\Delta\sigma_{c,P}$ is larger than $\Delta\sigma_{d,P}$, so that σ_P of the convex side CFRP is zero. As the lateral displacement increases, the lateral bending phase occurs, and $\Delta\sigma_{d,P}$ is the major stress change, so the convex side CFRP stress starts to increase. Because there is no prestressing chair in these cases, there is no transverse force S at the midspan (see Fig. 1). Therefore, the CFRP cannot provide lateral support against buckling and only slightly enlarges the steel section area. Thus, the reinforcing efficiency of the S specimens is very limited.

Based on the steel stress change, for the S specimens, the critical states of (3) buckling and (4) steel column edge yielding occur at the same time. Thus, the buckling of the S specimens is controlled by the yielding of the steel material; this scenario is the same as that observed for the pure steel column.

4.3.2. PS specimens

For the PS specimens, the measured CFRP stress ($\sigma_{PS,P}$) and steel stress ($\sigma_{PS,s}$) and the calculated S and N values with lateral displacement curves are shown in Table 4 and Figs. 18 and 19. The angle α is considered as unchanged.

For specimen I105-PS, after the prestressing and before loading, the CFRP stress ($\sigma_{PS,P}$) is 123 MPa. Through calculation, S_l and S_r are both 1.1 kN; thus, S is 0, N is 36.8 kN, and N allows the steel section to bear 30.2 MPa of compressive stress. In the beginning of loading, corresponding to the compressive deformation phase, because the lateral deformation is not very large, $\Delta\sigma_c$ is the dominant stress compared with $\Delta\sigma_d$, so the entire column is compressed, and the stress of both CFRPs decreases. After the lateral displacement toward the right side reaches a certain threshold, the lateral deformation phase occurs, and $\Delta\sigma_d$ becomes the dominant stress, so the stress of the right side CFRP continues to increase, while the stress of the left side CFRP continues to decrease. Before buckling, both CFRPs are under tension, which causes the difference between S_l and S_r to continue to increase from zero at a constant rate during the loading procedure. S reaches 2.0 kN when buckling occurs, which effectively delays the lateral deformation. After the slacking of the concave side CFRP, the rate of increase in S suddenly decreases because slack CFRP cannot provide a negative force to drag the steel column. Throughout the loading procedure, N first decreases and then increases, and the inflection point occurs when the concave side CFRP becomes slack. After the inflection point, N has a positive correlation with S. N reaches 15.9 kN when buckling occurs, which is 6.4% of the buckling capacity P_b. The steel stress changes accordingly. In the compressive deformation phase, the stress of the whole section decreases; in the lateral deformation phase, the stress of the tensile side begins to increase until reaching the yield point, while the stress of the neutral axis and the compression side continues to decrease.

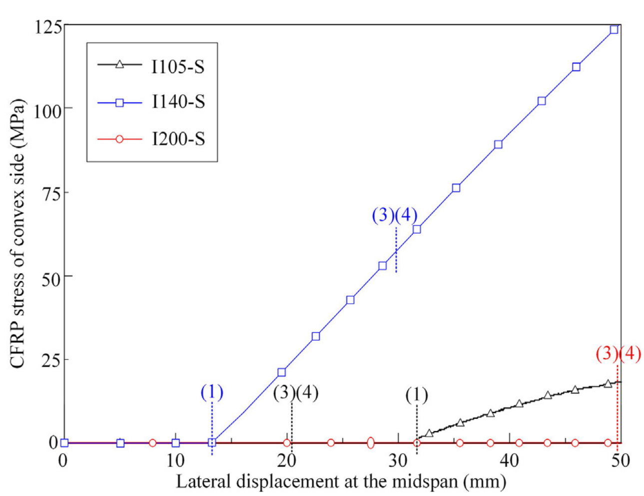

Fig. 17. Critical states and CFRP stress-lateral displacement curves of the S specimens.

Specimens I140-PS and I200-PS have a similar tendency as that of specimen I105-PS. Without providing the details of the similarity, three main differences are discussed here. First, the CFRP stress/S/N/steel stress after prestressing and those when buckling is triggered are different. For I140-PS, after prestressing and before loading, $\sigma_{PS,P}$ is 302 MPa, T_i is 45.3 kN, $S_l(=S_r)$ is 3.3 kN, S is 0 and N is 90.4 kN, causing the steel section to bear 74.1 MPa of compressive stress. When buckling occurs, S reaches 3.0 kN, and N reaches 49.8 kN (19.3% of P_b). For I200-PS, after prestressing and before loading, $\sigma_{PS,P}$ is 146 MPa, T_i is 21.9 kN, $S_l(=S_r)$ is 1.3 kN, S is 0 and N is 43.7 kN, causing the steel section to bear 35.8 MPa of compressive stress. When buckling occurs, S reaches 1.5 kN, and N reaches 26.0 kN (21.3% of P_b). Second, unlike I105-PS, the CFRP stress of I200-PS only decreases slightly and then increases. This is because for steel columns that are very slender, the compressive deformation phrase is relatively short, so the lateral deformation phrase arrives very quickly.

For specimens in the eccentric loading group, the CFRP stress/steel stress/S/N change trends are basically the same as those of the specimens in the axial loading group. However, the results of the eccentric loading group do not have a compressive deformation phase. This is because under eccentric loading, lateral deformation develops much faster than axial deformation; thus, $\sigma_{c,P}$ is always smaller than $\sigma_{d,P}$. Specifically, there is no stage of stress decrease for the convex side CFRP, and the concave side CFRP stress starts to decrease when there exists a lateral displacement. Therefore, the time of the slacking of the concave side CFRP is later than that for the specimens tested under axial compression, leading to later buckling with a larger deformation and larger values of S and N than those of the specimens tested under axial compression. In addition, the steel stress of the tension side at the midspan continues to increase, that of the neutral axis remains basically unchanged and that of the compression side continues to decrease.

Most notably, the slacking of the concave side CFRP corresponds to an important moment. S continues to increase, but its rate of increase suddenly decreases at this moment; N transitions from increasing to decreasing at this moment. Thus, the slacking of the concave side CFRP actually causes a sudden change in the boundary conditions of the steel column. Therefore, for the PS specimens, slacking of the concave side CFRP is defined as one of the 4 possible critical states.

The order of the 4 possible critical states of all the PS specimens is summarized here, among which specimens in the axial loading group are shown in Fig. 20. The I105-PS specimen is similar to the S specimens, which first experience the slacking of the concave side CFRP and then buckle when the steel yields. However, unlike the S specimens, for the I140-PS and I200-PS specimens, the buckling and slacking of the CFRP occur in close succession, and no yielding of the midspan of the steel column is observed. The situations among the specimens in the eccentric loading group also vary. I105-PS-e0 exhibits the largest CFRP prestress, which buckles just after the slacking of the concave side CFRP, without any signs of steel yielding. I105-PS-e1 exhibits the second-largest CFRP prestress, which experiences the slacking of the concave side CFRP and buckling and edge yielding of the steel section at the midspan. I105-PS-e2 and I105-PS-e3 have a small CFRP prestress, which both first experience the slacking of the concave side CFRP and then undergo buckling and midspan steel yielding (or almost yielding) at the same time.

Table 4
Details of the stress states before loading and buckling.

Specimen		After prestressing and before loading				Buckling	
		$\sigma_{PS,P} = T_i/A_P$ (MPa)	$S_l = S_r$ (kN)	N (kN)	$\sigma_{PS,s} = -N/A_s$ (MPa)	S (kN)	N (kN)
Axial loading group	I105-PS	123	1.1	36.8	−30.2	2.0	15.9
	I140-PS	302	3.3	90.4	−74.1	6.0	49.8
	I200-PS	146	1.3	43.7	−35.8	3.0	26.0
Eccentric loading group	I105-PS-e0	190	2.2	56.8	−46.6	5.2	33.8
	I105-PS-e1	220	2.7	65.8	−53.9	9.4	57.7
	I105-PS-e2	160	1.9	47.9	−39.2	9.8	62.8
	I105-PS-e3	150	1.7	44.9	−36.8	9.6	64.1

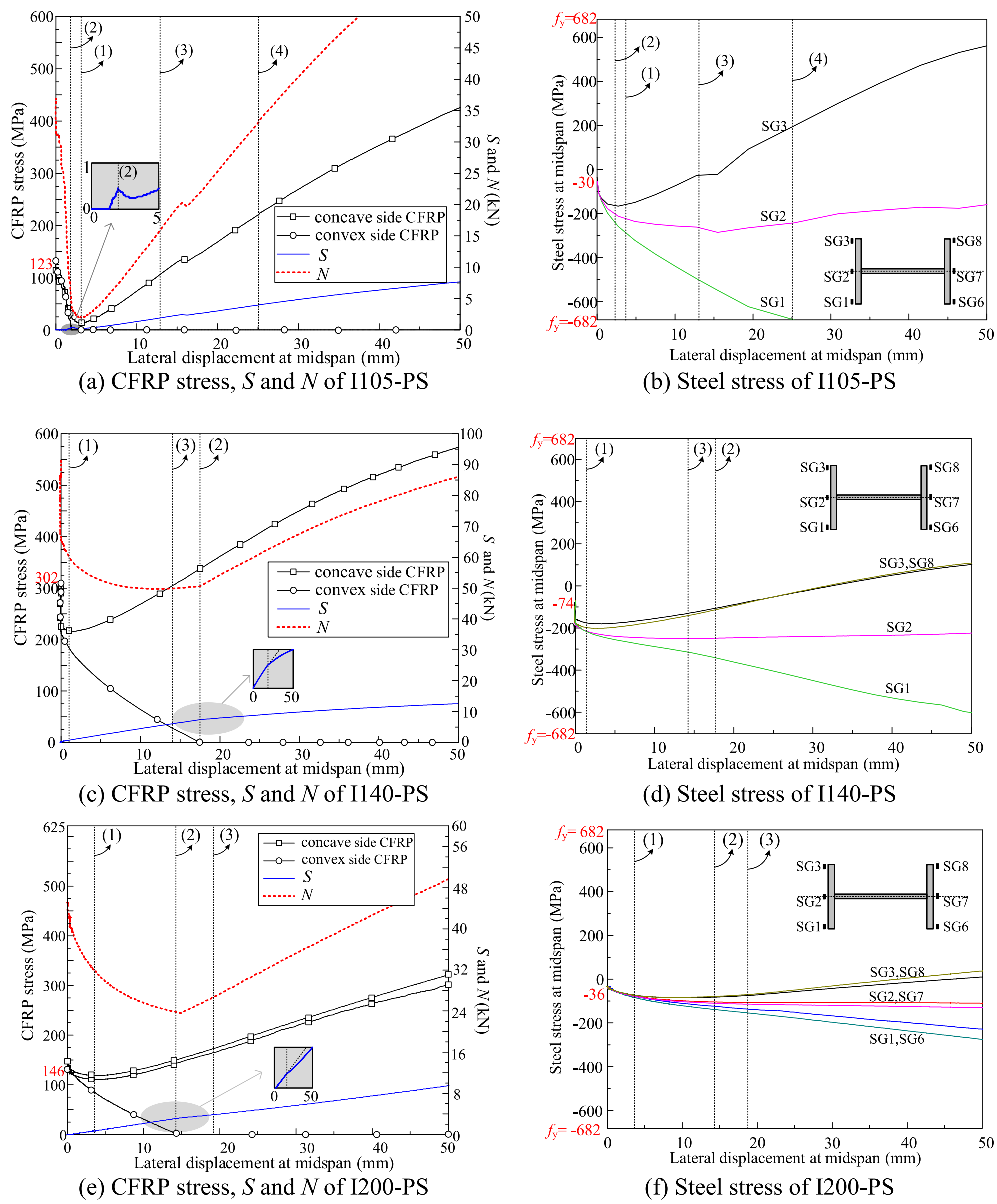

Fig. 18. Critical states and CFRP stress/S/N/steel stress-lateral displacement curves of the PS specimens in the axial loading group.

Thus, the buckling of I140-PS, I200-PS, I105-PS-e0 and I105-PS-e1 is caused by the slacking of the concave side CFRP, and the buckling of I105-PS, I105-PS-e2 and I105-PS-e3 is caused by the yielding of the material. Since the steel stress was measured only at the midspan, to determine the accurate stress of each section of the steel column when buckling is triggered and thus study the reasons for the buckling of all the specimens, FEM and a theoretical analysis will be utilized in the future.

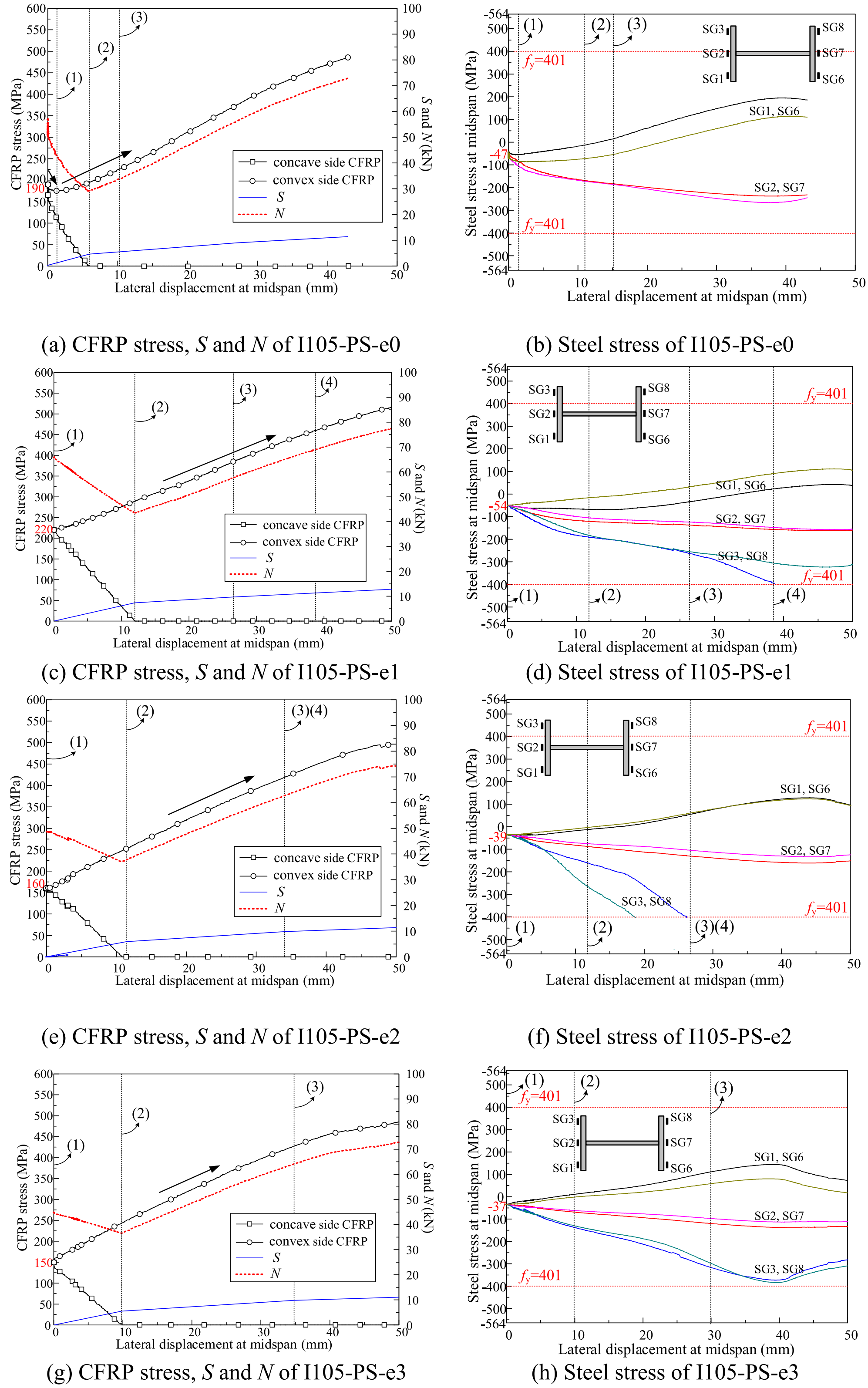

Fig. 19. Critical states and CFRP stress/*S*/*N*/steel stress-lateral displacement curves of the specimens in the eccentric loading group.

5. Simplified model of reinforcing efficiency

Based on current test results, a simplified model of reinforcing efficiency can be preliminarily built. The reinforcing efficiency ($P_{b,s}/P_{b,u}$) is influenced by the ratio of the final supporting length to the steel column length a/L, the ratio of the initial supporting length to the steel column length a_0/L, the steel column slenderness λ, the ratio of the CFRP stiffness to the steel column stiffness $E_PA_P/(L_P + 2L_a)/(E_sA_s/$

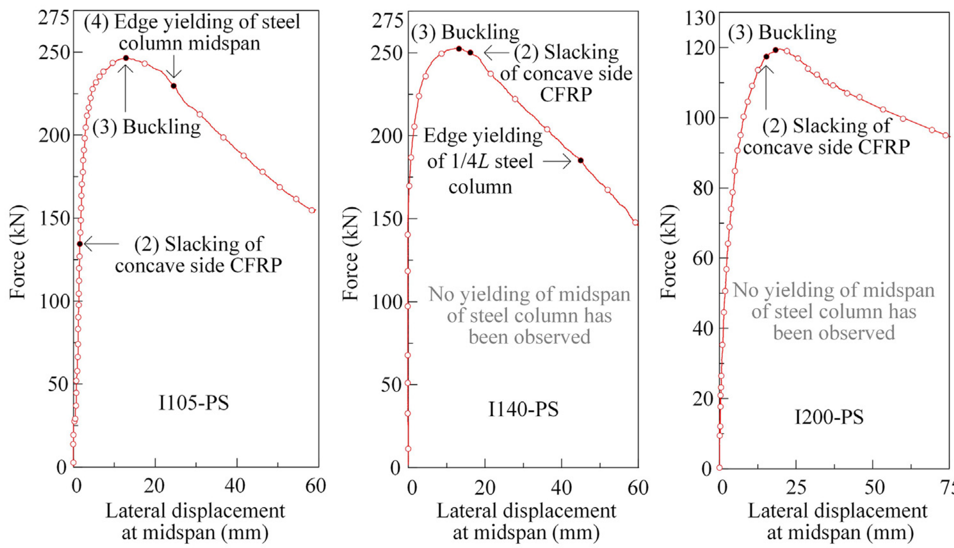

Fig. 20. Critical states in the force-lateral displacement curve of specimens in the axial loading group.

L), the eccentric ratio e/r, the yield point of steel f_y, the steel column initial imperfection at midspan v_{om}, etc. Thus, a function can be built in the form of Eq. (7).

$$P_{b,s}/P_{b,u} = \text{Function}(x1, x2, x3, \ldots, x7) = \text{Function}\left(a/L, a_0/L, \lambda, \frac{E_P A_P/(L_P + 2L_a)}{E_s A_s/L}, e/r, f_y/235, v_{om}/L\right) \tag{7}$$

The influence of some of the abovementioned parameters on the reinforcing efficiency is shown in Figs. 7 and 8.

Based on Fig. 7, comparing I105-PS and I200-PS with the same a/L but different slenderness, the reinforcing efficiency of I200-PS (2.18) is much higher than that of I105-PS (1.36). It can be inferred that a steel column with a large λ can achieve a high reinforcing efficiency when all the other parameters are the same. Additionally, because I140-PS has a moderate slenderness but the highest reinforcing efficiency (2.50), it can be inferred that a large a/L is beneficial to the reinforcing efficiency.

Based on Fig. 8, with a very similar a/L ratio, as the eccentricity increases, the buckling capacity decreases, and the reinforcing efficiency increases. There are two reasons for this phenomenon. First, because of the eccentricity, the buckling capacities of the U specimens decrease considerably, which improves the reinforcing efficiency. Second, under eccentric loading, when the other conditions remain constant, the stress of the convex side CFRP does not decrease but increases rapidly from the beginning of the test with the development of the midspan lateral displacement. This makes the PS CFRP provide a larger transverse force S when buckling occurs, thus leading to a higher buckling capacity. The relationship of e/r and reinforcing efficiency can be quantitatively fitted according to test results, as shown in Fig. 21. Thus, Eq. (8) is obtained.

$$\text{Function}(3.2\%, 0, 105, 0.12, e/r, 1.71, 0.02) = 0.0047e/r + 1.16 \tag{8}$$

Furthermore, comparing specimens I105-PS-e0 and I105-PS can lead to the following conclusion: I105-PS has an a/L value of 2.5%, and its buckling capacity is improved by 66% by PS CFRP. I105-PS-e0 has an a/L value of 3.2%; however, its buckling capacity is only improved by 19% by PS CFRP. This difference is because the steel yield point of I105-PS is 682 MPa, which is larger than that of I105-PS-e0 (401 MPa). Thus, it can be concluded that a high yield point f_y leads to a high reinforcing efficiency.

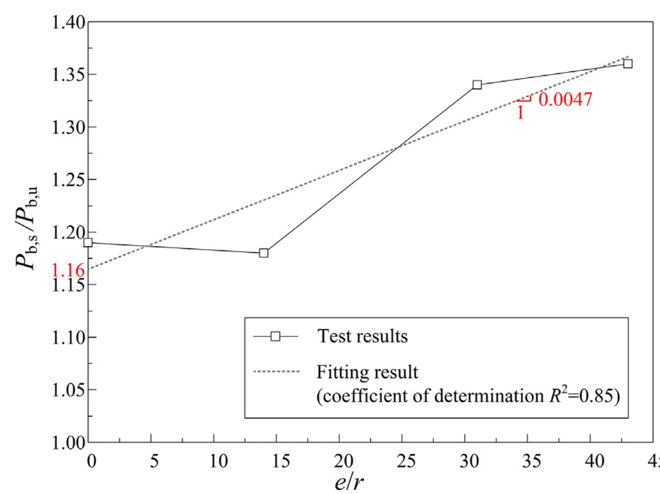

Fig. 21. Fitting result of the relationship of e/r and reinforcing efficiency.

From this testing, the influencing tendency of other parameters has not been obtained and needs to be further studied by conducting more tests and finite element calculations. With the results of that work, this model could be improved and completed.

6. Conclusions

By performing compression tests of 12 steel columns of 3 forms (U, S and PS), 3 slenderness values (105, 140, and 200) and 4 different eccentric ratios (0, 1, 2, and 3), the reinforcing efficiency, parameter influencing tendency, and failure mode and mechanism of PS CFRP-reinforced steel columns are obtained and analyzed in detail. The following conclusions are drawn:

(1) PS CFRP reinforcing of steel columns can achieve a good reinforcing efficiency. The reinforcing efficiency ranges from 1.36 to 2.50 under axial compression and 1.19 to 1.36 under eccentric compression in these tests. In addition, PS CFRP reinforcing can significantly improve the bending stiffness of steel columns under axial and eccentric compression.

(2) Failure modes are obtained. For all the specimens, CFRP does not rupture or debond before buckling occurs. Notably, the failure modes of the U, S and PS specimens are different. For all the U and S specimens, typical symmetric buckling occurs. For the PS specimens with a small value of a/L, symmetric buckling occurs at the peak load, followed by asymmetric deformation; for the PS specimens with a large value of a/L, mixed buckling occurs at the peak load, which is asymmetric deformation.
(3) The entire loading procedure is analyzed in detail, and the mechanism of effective reinforcing efficiency by PS CFRP is revealed. First, the rules of the CFRP and steel stress changes are obtained. Axial compression PS specimens have a compressive deformation phase and lateral deformation phase, while eccentric compression PS specimens only have a lateral deformation phase. Second, the transverse force S and vertical force N changes of all the specimens are analyzed. The slacking of the concave side CFRP is important because it causes a sudden change in the boundary conditions of the steel column. Thus, it is summarized that there are 4 possible critical states for PS specimens: the beginning of the lateral bending phase, slacking of the concave side CFRP, overall buckling, and steel column edge yielding. The order of the 4 critical states determines the cause of buckling, which is either the yielding of the material or the slacking of the concave side CFRP. Further research is needed to identify the essential reason for different causes of buckling.
(4) A simplified model of reinforcing efficiency is preliminarily built based on test results as a function of the ratio of the final supporting length to the steel column length, the ratio of the initial supporting length to the steel column length, the steel column slenderness, the ratio of the CFRP section stiffness to the steel section stiffness, the eccentric ratio, the steel yield point, the steel column initial imperfection, etc. To complete the model, the influencing tendencies of some parameters are obtained by fitting the test results, which helps to provide references for future design guidelines.

CRediT authorship contribution statement

Lili Hu: Data curation, Analysis, Investigation, Methodology, Writing - review & editing. **Peng Feng:** Conceptualization, Resources, Funding acquisition, Project administration, Writing - review & editing, Supervision.

Declaration of Competing Interest

The authors declare that they have no known competing financial interests or personal relationships that could have appeared to influence the work reported in this paper.

Acknowledgements

This research was supported by the National Key Research and Development Program of China (No. 2017YFC0703000), the National Natural Science Foundation of China (No. 51522807), and funding provided by Shanghai Jiao Tong University.

References

[1] Shaat A. Structural behaviour of steel columns and steel-concrete composite girders retrofitted using CFRP [Theses and Dissertations]. Queen's University; 2007.
[2] Teng JG, Hu Y. Behaviour of FRP-jacketed circular steel tubes and cylindrical shells under axial compression. Constr Build Mater 2007;21(4):827–38.
[3] Gao XY, Balendra T, Koh CG. Buckling strength of slender circular tubular steel braces strengthened by CFRP. Eng Struct 2013;46:547–56.
[4] Shaat A, Fam AZ. Slender steel columns strengthened using high-modulus CFRP plates for buckling control. J Compos Constr 2009;13(1):2–12.
[5] Feng P, Zhang Y, Bai Y, Ye L. Strengthening of steel members in compression by mortar-filled FRP tubes. Thin-Wall Struct 2013;64(3):1–12.
[6] Feng P, Zhang Y, Bai Y, Ye L. Combination of bamboo filling and FRP wrapping to strengthen steel members in compression. J Compos Constr 2013;17(3):347–56.
[7] Miller TC, Chajes MJ, Mertz DR, Hastings JN. Strengthening of a steel bridge girder using CFRP plates. J Bridge Eng 2001;6(6):514–22.
[8] Tavakkolizadeh M, Saadatmanesh H. Fatigue strength of steel girders strengthened with carbon fiber reinforced polymer patch. J Struct Eng 2003;129(2):186–96.
[9] Schnerch D, Rizkalla S. Flexural strengthening of steel bridges with high modulus CFRP strips. J Bridge Eng 2008;13(2):192–201.
[10] Hu L, Zhao XL, Feng P. Fatigue behavior of cracked high-strength steel plates strengthened by CFRP sheets. J Compos Constr 2016;20(6):04016043.
[11] Feng P, Hu L, Zhao XL, Cheng L, Xu S. Study on thermal effects on fatigue behavior of cracked steel plates strengthened by CFRP sheets. Thin-Wall Struct 2014;82:311–20.
[12] Ghafoori E, Motavalli M, Botsis J, Herwig A, Galli M. Fatigue strengthening of damaged metallic beams using prestressed unbonded and bonded CFRP plates. Int J Fatigue 2012;44:303–15.
[13] Abdollahi Chahkand N, Zamin Jumaat M, Ramli Sulong NH. Experimental and theoretical investigation on torsional behaviour of CFRP strengthened square hollow steel section. Thin-Wall Struct 2013;68:135–40.
[14] Wu C, He L, Ghafoori E, Zhao XL. Torsional strengthening of steel circular hollow sections (CHS) using CFRP composites. Eng Struct 2018;171:806–16.
[15] Hatami F, Ghamari A, Rahai A. Investigating the properties of steel shear walls reinforced with carbon fiber polymers (CFRP). J Constr Steel Res 2012;70:36–42.
[16] Nateghi-Alahi F, Khazaei-Poul M. Experimental study of steel plate shear walls with infill plates strengthened by GFRP laminates. J Constr Steel Res 2012;78:159–72.
[17] Zhao XL. FRP-strengthened metallic structures. Boca Raton, Florida: CRC Press; 2013.
[18] Feng P, Hu L. Steel columns strengthened/reinforced by prestressed CFRP strips: concepts and behaviors under axial compressive loads. Compos Struct 2019;198:109527.
[19] Chu K-H, Berge SS. Analysis and design of struts with tension ties. J Struct Div 1963;89(1):127–64.
[20] Smith RJ, McCaffrey GT, Ellis JS. Buckling of a single-crossarm stayed column. J Struct Div 1975;101(1):249–68.
[21] Hafez HH. Pretensioning of single-crossarm stayed columns. J Struct Div 1979;105 (2):359–75.
[22] Saito D, Wadee MA. Post-buckling behaviour of prestressed steel stayed columns. Eng Struct 2008;30(5):1224–39.
[23] Serra M, Shahbazian A, Silva LSD. A full scale experimental study of prestressed stayed columns. Eng Struct 2015;100:490–510.
[24] Feng P, Zou YC, Hu L, Liu TQ. Use of 3D laser scanning on evaluating reduction of initial geometric imperfection of steel column with pre-stressed CFRP. Eng Struct 2019;198:109527.
[25] Metallic materials-tensile testing-Part 1: method of test at room temperature, GB/T 228.1-2010; 2010 [in Chinese].
[26] Standard for design of steel structures, GB50017-2017; 2017 [in Chinese].
[27] Ribeiro D, Calçada R, Ferreira J, Martins T. Non-contact measurement of the dynamic displacement of railway bridges using an advanced video-based system. Eng Struct 2014;75:164–80.
[28] Chan SL, Shu GP, Lü ZT. Stability analysis and parametric study of pre-stressed stayed columns. Eng Struct 2002;24(1):115–24.
[29] Saito D, Wadee MA. Numerical studies of interactive buckling in prestressed steel stayed columns. Eng Struct 2009;31(2):432–43.
[30] Osofero AI, Wadee MA, Gardner L. Experimental study of critical and post-buckling behaviour of prestressed stayed columns. J Constr Steel Res 2012;79:226–41.
[31] Feng P, Cheng S, Bai Y, Ye L. Mechanical behavior of concrete-filled square steel tube with FRP-confined concrete core subjected to axial compression. Compos Struct 2015;123:312–24.